Earth and Planetary Science Letters 285 (2009) 124–130

Contents lists available at ScienceDirect

Earth and Planetary Science Letters

journal homepage: www.elsevier.com/locate/epsl

Thermal imaging of alluvial fans: A new technique for remote classification of sedimentary features

Craig Hardgrove [a,*], Jeffrey Moersch [a], Stephen Whisner [b]

[a] University of Tennessee, Department of Earth and Planetary Sciences, 1412 Circle Dr., Knoxville, TN 37926, United States
[b] Bloomsburg University of Pennsylvania, Department of Geography and Geosciences, 400 East 2nd St., Bloomsburg, PA 17815, United States

ARTICLE INFO

Article history:
Received 27 October 2008
Received in revised form 28 May 2009
Accepted 3 June 2009
Available online 5 July 2009

Editor: T. Spohn

Keywords:
alluvial fans
remote sensing
thermal infrared
debris flows
thermal inertia

ABSTRACT

We evaluate the utility of remote thermal image data for mapping geomorphic features and evidence of sedimentary processes on the surfaces of alluvial fans. Prior studies of alluvial fans have made extensive use of visible images and traditional field-based techniques. As a case study demonstration of this technique, we compare thermal images acquired from the ground and a light aircraft (altitude ~5000 ft) to a pre-existing ground-based map of features on the Dolomite Fan in Owens Valley, California. Thermal images from the aircraft were acquired at several times of day to determine how the surface temperatures of the alluvial fan rise and fall throughout a diurnal cycle. We have also acquired thermal images from the ground at 5 minute intervals over the course of a diurnal cycle. The aerial thermal images (ground resolution ~2 m/pixel) reveal evidence of a variety of sedimentary processes that have acted on the fan surface. These images show spatial–thermophysical patterns associated with clast-rich and clast-poor debris flows, debris-flow levees and the change in particle size at the toe of the fan. The locations of these features in the thermal images match the locations of the features previously mapped by others using traditional ground-based field sedimentology techniques. All debris flows that are exposed at the fan surface are evident in the aerial thermal images, including those that have been heavily weathered and are difficult to observe in visible images. This case study demonstrates that aerial thermal images can be used to provide reconnaissance of an alluvial fan, suggest what sedimentary processes have most recently acted on the surface of the fan, and to prioritize sites for detailed study on the ground.

1. Introduction

Alluvial fans form where high-gradient, confined, sediment-laden streams empty sub-aerially onto low-gradient, unconfined surfaces. The abrupt decrease in competence and capacity associated with the loss of stream energy at the break in slope results in deposition of sediments that build the fan. Within this general depositional context, smaller-scale depositional and erosional processes act to distribute the sediment along the fan surface in patterns characteristic of the sedimentary process that transported them. The purpose of the present study is to demonstrate the utility of using thermal infrared images for remote mapping of these features. We demonstrate that spatial–thermophysical patterns are representative of sedimentary processes that are observable at the surface of an example alluvial fan. This is accomplished through comparison of our remotely-acquired thermal images to a pre-existing ground-based map of the Dolomite Fan in Owens Valley, California (Blair and McPherson, 1998).

In an arid climate with low vegetation cover, the temperature of a surface at any given time of day is a complex function of many parameters, including slope, azimuth, composition, degree of induration, and particle size. By analyzing the temperatures on the surface of an alluvial fan with comparable slopes, azimuth, and composition, we make estimates of the relative particle size or degree of induration. We utilize the fact that several sedimentary processes acting on the surface of alluvial fans sort particles by size. For example, both debris flow and channelized flow processes can form lobate features of large and small clasts. Therefore, thermal images could be expected to reveal evidence of these processes at the surfaces of alluvial fans in the form of spatial patterns of thermophysical properties. Additionally, the use of remotely-acquired thermal data allows us to study sedimentary processes on alluvial fans where ground truth data are not available. This has the potential to be particularly useful in mapping sedimentary processes on Mars, where many alluvial fans have been proposed by others (*e.g.* Moore et al., 2003; Malin and Edgett, 2003; Kraal, 2008).

* Corresponding author. Tel.: +1 865 748 3837.
E-mail address: chardgro@utk.edu (C. Hardgrove).

0012-821X/$ – see front matter © 2009 Elsevier B.V. All rights reserved.
doi:10.1016/j.epsl.2009.06.004

2. Background

2.1. Sedimentology of fans

The type of particle-size distribution found on alluvial fans is primarily related to both the sediment source and the sedimentary processes that have acted on the fan. Fan particle-size distributions are complicated, but there is a nominal trend toward larger particles (sometimes called "fanglomerates") in the upper fan, intermediate particle sizes in the mid-fan, and smaller particles in the distal fan, or fanbase (Boggs, 2001). Upper fan particle sizes can be as large as boulder-sized, and distal fan particle sizes can be sand-sized or smaller (Blissenbach, 1952). However, this conceptualization is over-simplified for most alluvial fans, as their surfaces are often reworked by overland water flow and winnowing of fines by aeolian processes. The alluvial fan is primarily composed of sediment from major, yet infrequent events that deposit the majority of fan sediments. Debris flows, incised channel floods, and sheetfloods are examples of processes that deposit large quantities of fan sediment. These large-scale deposits can then be reworked by decades of small-scale surface modification by rainfall or wind blown sand (Blair and McPherson, 1994). The surface particle-size distribution will be representative of both the large-scale depositional processes and the reworking by smaller-scale weathering processes.

Blair and McPherson (1994) studied the sedimentary processes that operated on alluvial fans in detail. They showed that sediments deposited by debris flows can be either clast-rich or clast-poor and will overlie pre-existing surface features. Clast-rich debris flows deposit a large percentage of the coarse component at the surface. They will also form debris-flow levees, which are paired linear features that lie on opposite margins of the debris flow. Prolonged exposure to surface weathering processes will winnow away the finer components of the clast-rich debris flow and what remains will be the largest particle-size component, forming an outline of the remnant debris flow. Clast-poor debris flows tend to form during the waning stage of a depositional event and leave a thin mantle of fines that drape over pre-existing deposits. Incised channel deposits tend to sort material within the channel into larger particle sizes near the center of the channel and smaller particle sizes along the margins of the channel. On many fans, repeated annual overland flow or aeolian activity will result in a sandskirt of fine material at the toe of the alluvial fan. Although the absolute particle sizes in these deposits can vary from fan to fan due to differences in source material, relative particle-size patterns are consistent.

2.2. Thermophysical remote sensing

Thermal inertia, I, can be thought of as a surface's ability conduct and store heat during the day and re-radiate it away at night in the thermal infrared portion of the spectrum. It is defined as $I=(k\rho C)^{1/2}$, where k is the thermal conductivity, ρ is the bulk density, and C is the specific heat capacity of the surface (Kieffer et al., 1977). Thermal inertia has two primary effects on the shape of a surface's diurnal temperature curve. First, all other factors being equal, a low thermal inertia surface will experience higher peak temperatures and lower minimum temperatures than a high thermal inertia surface because the low thermal inertia surface heats and cools faster. Second, the time of day at which a low thermal inertia surface experiences its peak temperature will be close to local solar noon, whereas a high thermal inertia surface may not reach its peak until later in the afternoon. Surface slope and azimuth can also change diurnal temperature curves, as these variables affect the amount and timing of insolation the surface receives over a day–night cycle. A reasonable first order approximation to remove these geometric effects is to observe temperatures in the pre-dawn hours, when the effects of topography are muted. Another advantage of pre-dawn observations is that surfaces of different thermal inertias have cooled overnight at different rates, maximizing the variations in temperature between them (Watson, 1975; Watson, 1982; Colwell and Jakosky, 2002; Gupta, 2003).

For rocks and soils, bulk density (ρ) does not vary significantly. For a dry surface, the specific heat capacity (C) also does not vary significantly. Therefore, variations in thermal inertia are primarily due to variations in thermal conductivity (k) (*e.g.* Kieffer et al., 1977; Gupta, 2003). The primary controls on thermal conductivity of a dry surface are particle size and the degree of induration of the regolith (Kieffer et al., 1977). A surface composed primarily of bedrock or large ($>\sim$10 cm) rocks has a very high thermal inertia, whereas a thermally-thick regolith of fine-grained dust has a very low thermal inertia. In very fine regolith, thermal inertia is controlled by the efficiency of thermal conduction in the pore spaces between grains (Jakosky, 1986). At larger particle sizes, thermal inertia is controlled by the size of the particle compared to the diurnal thermal skin depth ($\sim$10 cm for rock). At particle sizes above this scale, all rocks begin to look like bedrock in terms of their thermal inertia. A well-indurated (*e.g.*, cemented) regolith of fine particles will have a thermal inertia more like solid rock than fines. In general, thermal inertia is sensitive to particle sizes ranging from dust size to cobble size.

It is important to note that diurnal temperature variations of geologic surfaces are not strongly influenced by the thermophysical properties of materials deeper than approximately one diurnal thermal skin depth (approximately 1 cm for sand and 10 cm for rocks, respectively). Therefore, thermal images are only useful for mapping sedimentary features at or near the surface. This means that the technique is not useful for characterizing the types of processes that have volumetrically dominated the construction of the fan (*e.g.*, identifying a fan as "debris-flow dominated" or "fluvially dominated"). Typically, only the most recent processes that have overprinted the fan will be evident.

3. Methods

All thermal image data were acquired with a FLIR Systems ThermaCam S45 thermal infrared camera. The camera operates in the 7.5–13-μm telluric transmissivity window, and has an absolute temperature accuracy of 2 K at ambient temperatures relevant for geologic studies. Relative pixel-to-pixel temperature accuracy is about 0.1 K. The field of regard is $24^\circ\times18^\circ$ across a 320×240 pixel array, giving the camera a pixel IFOV of 1.3 mrad. Images are captured at 60 Hz, which in practical terms means pixel blur from a light aircraft platform is not a problem at altitudes of about 3000 ft or greater above the terrain. The camera is able to auto-capture images at user-defined intervals, so that the camera need not be disturbed when taking time-sequences from a fixed location on the ground. We have written custom software that converts images from the manufacturer's digital image format into files for use in the Environment for Visualizing Images (ENVI) remote sensing software suite.

Thermal images are acquired in two different modes. For the first mode, time-lapse images are obtained by mounting the camera to a tripod on the ground at a position that allows the entire fan to fit within the camera's field of regard. Images in this mode are acquired at regular, short intervals (every few minutes) over the course of at least one diurnal cycle. Concurrent meteorological observations (air temperature, humidity, and barometric pressure) are made with a Nielson-Kellerman Kestrel 4000 pocket weather station. Images from the time-lapse sequence are stacked into a single data product called a hypertemporal image cube, in which two dimensions are the spatial dimensions of the scene and the third dimension is time of day. Temperature values extracted for a single spatial pixel along the time axis of this image cube comprise a diurnal thermal curve for that pixel's location.

The hypertemporal image cube of the target alluvial fan will display variations in diurnal temperature curves across its surface, as shown in Fig. 1. The two example pixels in Fig. 1 have significantly different diurnal temperature curves, representing two different

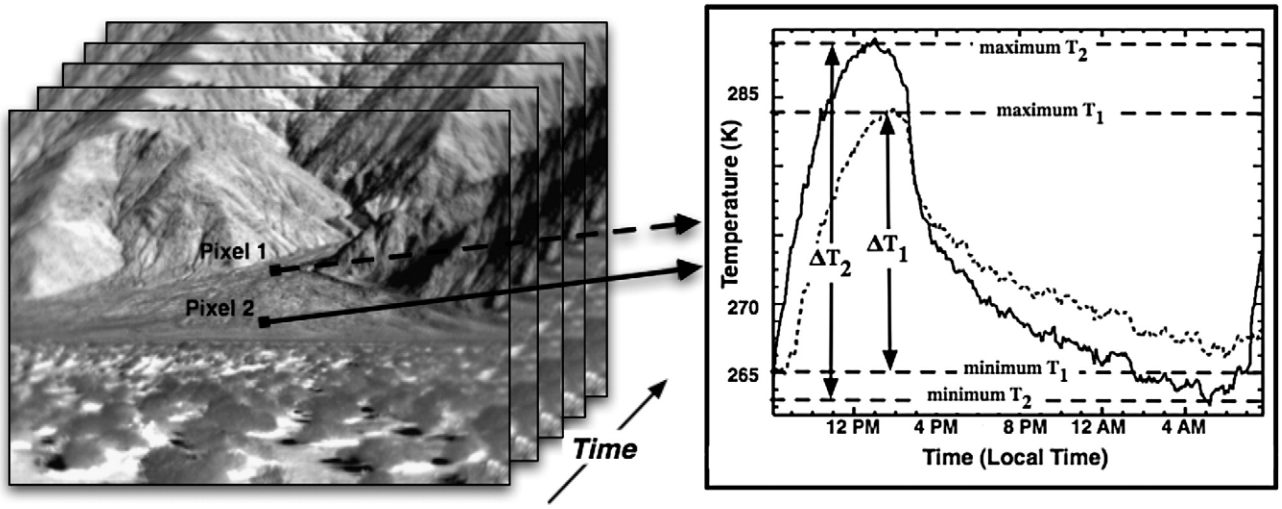

Fig. 1. (left) Representation of a hypertemporal image cube for the Dolomite Fan acquired from the ground over a 24-hour diurnal cycle. (right) Two example diurnal temperature curves are extracted from the image cube in areas of high thermal inertia (pixel 1 - dashed line) and low thermal inertia (pixel 2 - solid line).

thermal inertia surfaces. The higher thermal inertia (pixel 1 - dashed line) pixel displays a smaller day/night temperature change, is slower to rise in temperature after sunrise, and is slower to cool after the time of peak temperature. The lower thermal inertia (pixel 2 - solid line) pixel displays a larger day/night temperature change, quickly rises in temperature after sunrise and rises drop in temperature at time of peak temperature. Fig. 1 also shows that the greatest difference in temperature between the two pixels occurs in the pre-dawn hours and before local noon. These times of day provide the highest contrast thermal images for surfaces with different thermal inertias, therefore, they were used to determine our flight times for the second mode of operation.

In the second mode of operation, individual images of the target alluvial fan are acquired at selected times of day and night from a light aircraft to give an overhead perspective similar to that seen from orbit, but at higher spatial resolution. As with ground-based data, pre-dawn aerial images were found to be optimal for seeing contrasts in thermal inertia because topographic effects are muted at this time of day and surfaces with different thermal inertias have a relatively large spread in temperature (*e.g.* Gupta, 2003). Daytime thermal and visible images are also acquired during the same 24-hour period from the same airborne vantage points as the pre-dawn images by using an aviation GPS unit.

Sophisticated multivariable analytical models for the diurnal thermal behavior of terrestrial surfaces have been developed (*e.g.* Watson, 2000), but here we make the simplifying assumption that thermal inertia is inversely proportional to the change in surface temperature between pre-dawn and mid-day (ΔT). This assumption was necessary in acquisition of our aerial data because it was logistically impossible to acquire thermal images sampled frequently over the entire diurnal cycle. The ΔT approach affords us better separation between surfaces of different thermal inertias than would be available from a single temperature image because the temperatures of high vs. low thermal inertia surfaces trend in opposite directions in day vs. night images. Because the thermal radiance measured by the camera is non-linearly dependent on surface temperatures, mid-day thermal images are disproportionately sensitive to smaller grains that heat up quickly during the day and pre-dawn thermal images are particularly sensitive to larger grains that stay warmer at night. The ΔT image is therefore optimally sensitive to both larger and smaller grain sizes. The ΔT image also partially eliminates the effects of albedo on the diurnal temperature curve. Changes in albedo primarily shift the entire diurnal temperature curve up or down because of differences in how much insolation different albedo surfaces absorb (Fig. 2A). The primary effect on diurnal

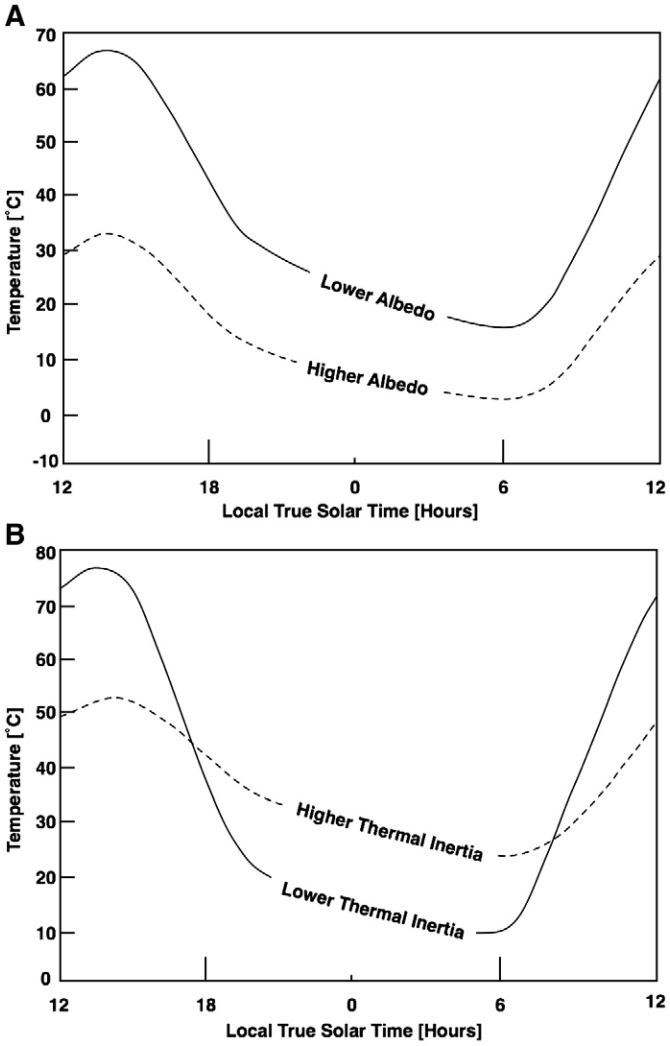

Fig. 2. Schematic diurnal temperature curves showing the effects of independently varying thermophysical properties (adapted from Watson, 1975). A) Diurnal temperature curves for two surfaces with the same thermal inertia, emissivity, insolation geometry and history, but with relatively low (solid curve) and high (dashed curve) albedos. B) Diurnal temperature curves for two surfaces with the same albedo, emissivity, insolation geometry and history, but with relatively low (solid curve) and high (dashed curve) thermal inertias.

thermal curves of differences in thermal inertia, on the other hand, is to change the total daily temperature swing of the surface (Fig. 2B). Therefore, by differencing the maximum and minimum temperature image, the ΔT image is sensitive primarily to the thermal inertia of the surface and not its albedo. Large-scale slope effects are reduced because the entire fan is generally oriented with surfaces facing to the west. As documented by Blair and McPherson, the fan has two discrete slope segments, where within those segments the slope is continuous. The overall average radial slope of the fan is 8.4° (Blair and McPherson, 1998). Smaller-scale slope effects and shadows are not taken into account, however, as will be seen, these approximations are adequate for revealing surface thermophysical heterogeneities associated with differences in particle size and/or induration in the scene. We note, however, that the ΔT image only allows for derivation of relative thermal inertias, not absolute thermal inertia values. Because of this, we make no attempt to derive absolute grain sizes from our remote datasets—only relative grain sizes are discussed.

To choose our two times of day for acquisition of aerial data, we used our ground-based hypertemporal image cube acquired at 5 minute intervals. We selected times of day during which surfaces of different thermal inertias had the greatest separation in temperature—3:30 to 5:00 AM local time for pre-dawn images and 11:00 to 12:30 AM local time for mid-day images. By co-registering and differencing the mid-day and pre-dawn aerial thermal images, we derive a new image in which pixel values approximate the diurnal change in temperature. Pixels with a high change in temperature contain relatively lower thermal inertia materials, and pixels with low temperature changes contain relatively higher thermal inertia materials. Because lower thermal inertias correspond to smaller particle sizes, the ΔT image shows the spatial distribution of relative particle sizes (or, in some areas of high thermal inertia, areas of induration). A 1st-order polynomial fit was used to warp the pre-dawn image to the mid-day image so that the image subtraction could be performed. The resulting error from the warping was +/−8 m/pixel, which represents the number of pixels that the pre-warped image deviates from the derived polynomial used for the warping.

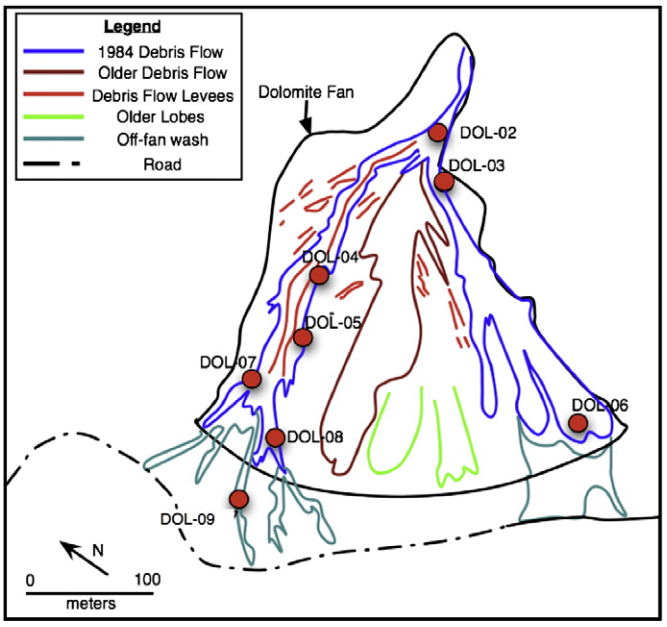

Fig. 4. Surface map of Dolomite Fan, adapted from Blair and McPherson (1998) field investigation. Red dots indicate the locations of ground stations where grain size measurements, shown in Table 1, were acquired by Blair and McPherson. Solid blue lines represent the recent, 1984 clast-rich debris flows. Solid maroon lines represent older, continuous clast-rich debris flows. Solid red lines represent debris-flow levees. Solid green lines represent older, discontinuous debris-flow lobes that have been eroded by subsequent debris flows or weathering processes. Solid turquoise lines represent off-fan wash, which we found commonly corresponds to clast-poor debris flows near the toe of the fan. The dashed black line represents a dirt road near the Owenyo Lone Pine Road at the toe of the Dolomite Fan.

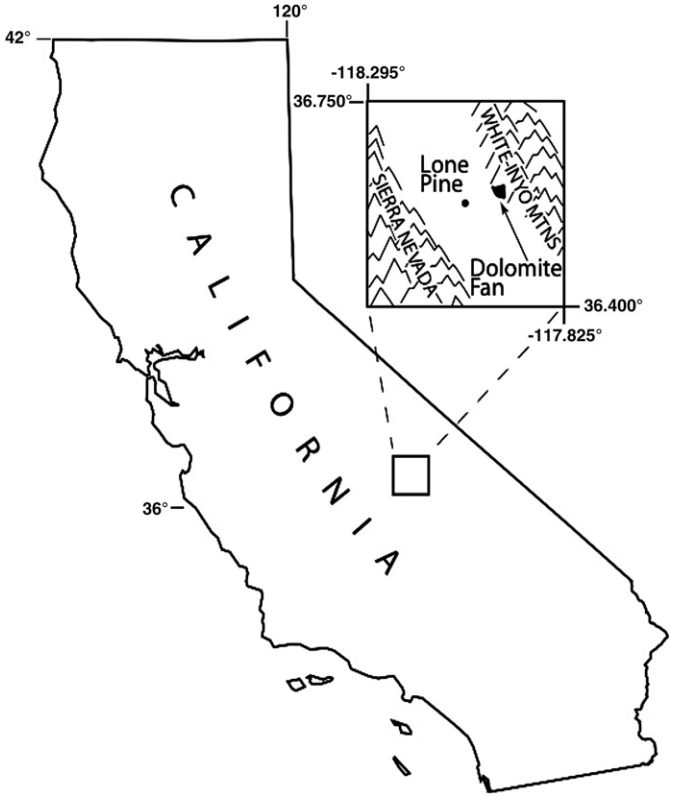

Fig. 3. Location map for the Dolomite Fan in Owens Valley, CA. The Dolomite Fan is located at approximately 36.6° N, 117.9° W.

4. Data

To test the methods described in Section 3, we have acquired data for the Dolomite Fan, which lies on the eastern side of Owens Valley in the arid southwestern United States Basin and Range extensional province (Fig. 3). This fan was chosen for our study because of extensive pre-existing characterization using traditional field methods by Blair and McPherson (1998). The Owens Valley is a north–south oriented extensional basin. It is a classic graben system with a down-dropped block forming the valley floor and uplifted rocks forming the high mountains bounding it (Pakiser et al., 1964). The eastern side of Owens Valley is bounded by the White-Inyo Mountains, which are composed of mixed lithologies as opposed to the primarily igneous lithology of the Sierra Nevada to the west (Bierman et al., 1991). Owens Valley is a good choice to test this new technique because it lies within the rain shadow of the eastern Sierra Nevada and receives water mostly in the form of infrequent thunderstorms or from snowmelt. This aridity minimizes vegetation and the effects of moisture on the fans studied.

The Dolomite Fan has a typical conical fan shape, an apex elevation of 1220 m and a maximum relief of 80 m. It is 515 m wide at its maximum extent, extends radially for about 540 m and covers an area of 0.26 km^2. The Dolomite Fan provides us with the opportunity to observe an alluvial fan that has undergone primary deposition in its recent history. This allows us to observe a relatively pristine alluvial fan surface, as it should appear with minimal reworking by secondary processes. In August, 1984, a multiphase debris flow was triggered by a thunderstorm in Owens Valley. The main deposition took place in two main debris flows on the northern and southern edges of the fan. The deposits vary in thickness from 10 to 300 cm and cover approximately 26% of the fan surface. The debris-flow levees and lobes created by the flow generally

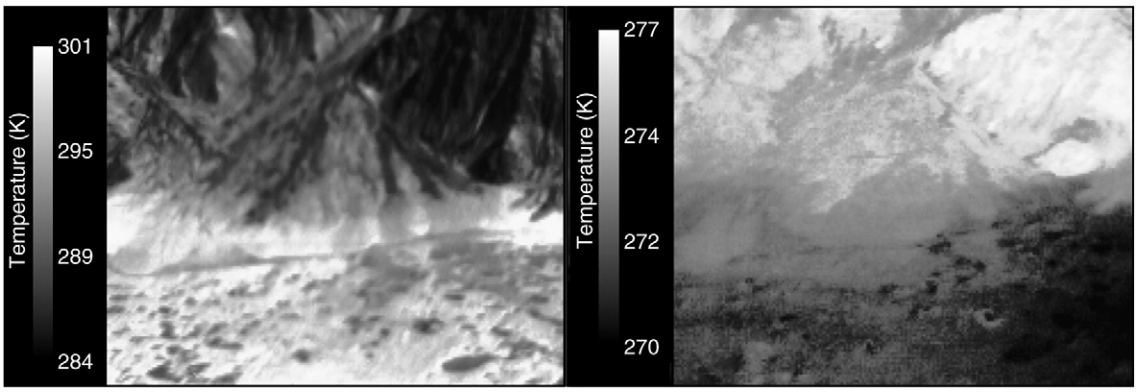

Fig. 5. Oblique viewing angle aerial thermal images show mid-day (*left*) and pre-dawn (*right*) temperatures of Dolomite Fan. The night temperature image has been geometrically registered to the mid-day temperature image.

consist of muddy, pebbly, and cobbly deposits, in varying proportions, leading to differences in average particle size. Debris-flow levees, which are found around the margins of the flows, tend to be predominately clast-supported and contain a higher fraction of boulders, giving them a relatively high average particle size. The debris flows interior to the levees are also clast-rich but matrix supported, giving them a somewhat lower average particle size. The distal ends of the clast-rich lobes are overlain by off-fan wash materials which are rich in mud, giving them a lower average particle size (Blair and McPherson, 1998).

Using a traditional field sedimentological approach, Blair and McPherson (1998) produced a surface map of the features on the Dolomite Fan (Fig. 4), which included the locations of both older and recent debris-flow lobes and levees, the off-fan wash and the break in slope near the toe of the fan. They performed particle-size measurements at 8 stations along the 1984 debris flows, which provide us with a means to verify our thermal image interpretations (Section 5).

We have acquired ground-based thermal images of the Dolomite Fan over the 24-hour period starting at 8 AM local time on December 30th, 2007. Images were collected at 5 minute intervals over the full diurnal cycle, resulting in 288 images containing ~2.3×10^7 individual temperature measurements. The stacked images were compiled into an 87 Mb hypertemporal image cube. Our aerial thermal images of the Dolomite Fan were acquired at 7:00 AM local time on March 29th, 2008 (just before sunrise) and 11:30 AM on the same day. Aerial visible images were acquired concurrently with the aerial mid-day thermal images. Fig. 5 shows the mid-day and pre-dawn thermal images of the fan. Fig. 6 shows the ΔT image, derived as described in Section 3. The corresponding visible image is shown in Fig. 7.

5. Analysis and interpretation

To evaluate the utility of our remote thermal imaging approach to mapping sedimentary processes on alluvial fans, we first validate the ability of the thermal data to distinguish different particle-size distributions by quantitatively comparing ΔT values from our images to particle-size measurements previously made on the ground using traditional sedimentological techniques. Then we qualitatively compare the spatial–thermophysical patterns seen in our thermal images with a surface feature map made on the ground.

The aforementioned particle-size measurements made at eight stations on the Dolomite Fan by Blair and McPherson (1998) consist of fractional abundances for three broad particle-size categories: gravel, sand, and mud (Table 1). Fig. 8 shows that there is a monotonic correlation between ΔT measurements from our images and the fractional abundance of mud (Fig. 8 *top*). There is also a monotonic inverse correlation between ΔT measurements from our images and the fractional abundance of gravel (Fig. 8 *bottom*). This demonstrates that our thermal difference images are sensitive to differences in particle-size distributions, as expected. A comparison of our ΔT measurements with Blair and McPherson's (1998) fractional abundances for sand (not shown) indicates that these parameters are not well-correlated. We speculate that the reason for this is that values in our ΔT image are largely determined by the extremes of the particle-size distribution, not the intermediate particle sizes. The total radiance captured in a given pixel is dominated by the warmest sub-pixel component due to the highly non-linear dependence of the Planck function on temperature. In the pre-dawn hours, the largest particle-

Fig. 6. ΔT image of Dolomite Fan calculated by differencing the pre-dawn and mid-day images in the previous figure. In this image pixel values approximate the diurnal change in temperature. Pixels with a high change in temperature contain relatively lower thermal inertia materials, and pixels with low temperature changes contain relatively higher thermal inertia materials. Because lower thermal inertias correspond to smaller particle sizes, this "delta-temperature" (ΔT) image shows the spatial distribution of relative particle sizes (or, in some areas of high thermal inertia, areas of induration).

Fig. 7. Oblique viewing angle aerial visible image of Dolomite Fan, taken from the same vantage point as the thermal images in Fig. 5. The light-toned features on the east (left) and west (right) margins of the fan are the 1984 clast-rich debris flows. The dark-toned feature in the mid-fan is an older debris flow. Other features, such as the clast-poor debris flows, remnant debris flows and levees are difficult to discern in this image while they represent prominent features in our ΔT image (Fig. 6).

size fraction (gravel) is warmest, contributing the most to the temperature reported in the thermal image. In the mid-day images, the smallest particle-size fraction (mud) is warmest and dominates. When the mid-day and pre-dawn images are combined to form a ΔT image, the effects of the smallest and largest particle sizes are emphasized, leading to the strong correlations observed in Fig. 8.

Qualitatively, there are many features in our ΔT image that correspond to the sedimentological features mapped on the ground by Blair and McPherson (1998) (Fig. 4). The darkest pixels (largest average particle size) on the alluvial fan in the ΔT image correspond to the debris flows in the Blair and McPherson map (regardless of age). These regions are outlined blue (for 1984 debris flow) and maroon (for older debris flow) in the annotated ΔT image shown in Fig. 9. Comparison of the thermal and visible images of the fan, Figs. 6 and 7, shows that only the young debris flows are clearly identifiable in the visible image, whereas the thermal image unambiguously shows both the younger and older debris flows. Older, more weathered debris flows that have had their fine component removed are seen in the thermal data as lobate rims of high thermal inertia features (low ΔT values). The off-fan wash deposits near the terminus of the southern debris flows, having smaller average particle sizes, are evidenced in the thermal data as areas of larger ΔT values (brighter pixels). Several, relatively dark, linear features appear in the ΔT image on and around the debris flows in locations where Blair and McPherson (1998) have mapped debris-flow levees. In Fig. 9 we have only labeled levees where they appear in pairs. Several of the debris-flow levees identified on the Blair and McPherson (1998) map are relatively small and may be unresolved in our thermal image. We note that the debris-flow levees that are most easily distinguished in our ΔT image are those associated with older debris flows. We speculate that this is because the aforementioned winnowing process has, over time, removed the fine components from these levees, leading to a contrast in particle-size distribution (and therefore ΔT) with the flows they surround. In order for thermal images to detect the levees there must be significant enough temperature contrast between the levee material and its surroundings. Modern debris-flow levees that lie on the margins of the 1984 debris-flow lobes cannot be readily identified in our thermal images, presumably because there is not yet sufficient particle-size contrast between these levees and the 1984 flow. The transition from clast-rich debris-flow lobes to clast-poor debris-flow lobes is clearly seen on the north and south sides of the fan. The lower thermal inertia (higher ΔT) clast-poor flows correspond to the "off-fan wash" materials mapped by Blair and McPherson (1998). Another spatial–thermophysical pattern displayed by the Dolomite Fan (Fig. 6) is a general trend toward lower thermal inertia (larger ΔT) at the distal

Table 1
Grain size data and ΔT data for Dolomite Fan.

Station	DOL-02	DOL-03	DOL-04	DOL-05	DOL-06	DOL-07	DOL-08	DOL-09
% Gravel	44	43	38	39	39	26	1	4
% Sand	26	27	27	28	26	30	41	30
% Mud	30	30	35	33	35	44	58	66
ΔT [K]	15.6	15.4	16.5	17.5	15.8	17.3	19.8	22.4

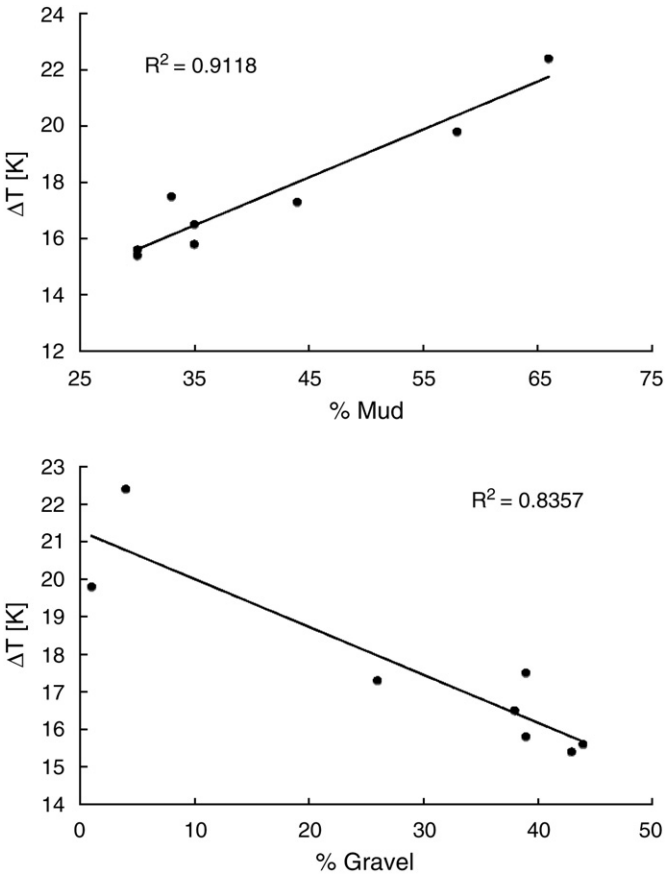

Fig. 8. Correlation between ΔT and fractional abundance of mud (*top*) and gravel (*bottom*) at 8 ground stations analyzed by Blair and McPherson (1998). Line is a calculated least squares regression through the data.

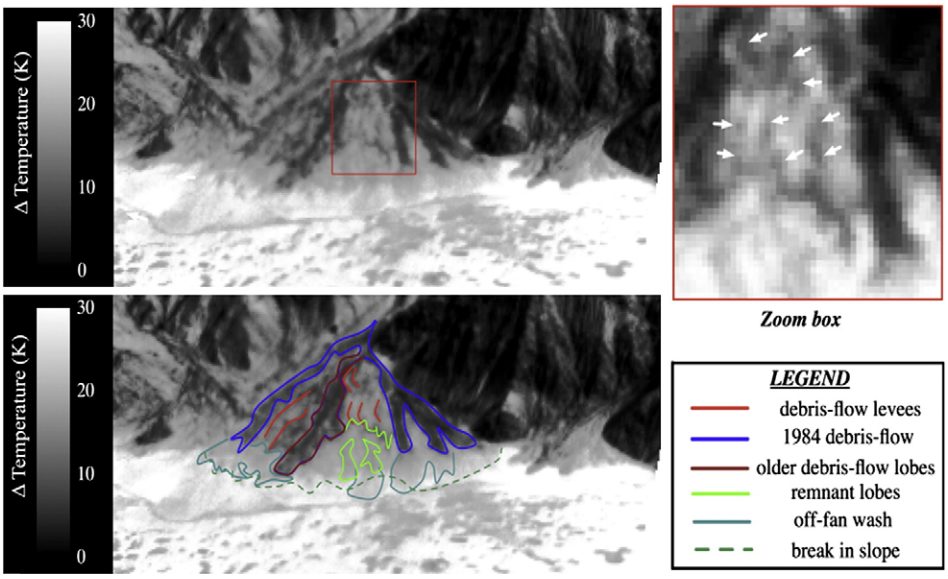

Fig. 9. ΔT image of Dolomite Fan with (bottom-left) and without (top-left) sedimentary features labeled. The zoom box (upper-right) shows the central debris flow (outlined in red in the top-left panel) as well as linear features that represent levees from remnant debris flows (white arrows).

margin of the fan. This pattern follows the general sorting trend displayed by most alluvial fans of depositing the finest particle-size fraction at the toe of the fan. Lastly, we note that there are several features revealed in the ΔT image, specifically, the low ΔT linear and lobate features in the bottom portion of the zoom box in Fig. 9, that do not correspond to any features mapped by Blair and McPherson (1998). These spatial–thermophysical patterns may be evidence of debris flows and other sedimentary features too subtle to be mapped using traditional ground-based techniques with no *a priori* knowledge of their existence, or it is possible they represent remnant features due to mid-day and pre-dawn thermal image registration. Such features would be excellent candidates for follow up field work.

6. Conclusions

The significant agreement between the thermal images presented here and the ground-based measurements presented by Blair and McPherson for the Dolomite Fan shows that remote thermal images offer a new way to perform initial reconnaissance of many sedimentary features on alluvial fans. Thermal images clearly show all debris flows that are exposed at the fan surface, even if the debris flows have been heavily weathered and are difficult to observe in visible images. Several other features can be identified, including the change in particle size at the toe of the fan, several thin clast-poor debris flows that extend beyond the clast-rich debris flows, and linear features that appear to be debris-flow levees.

High spatial resolution thermal images may be especially useful on Mars, where ground truth is not available, and where evidence for surface water and overland flow would be a significant result. For regions on Earth with very little near-surface moisture content, where the primary controls on surface temperature are particle size and degree of surface induration, thermal images can be used to provide a quick reconnaissance of alluvial fans, suggest what processes have most recently acted on the surface of a fan, and to prioritize sites for detailed study on the ground. Thermal images, when combined with ground measurements and visible images, are a useful tool for any geologist studying alluvial fans in an arid climate. Future work will expand our database of alluvial fans and the inventory of sedimentological features that can be identified with thermal images.

Acknowledgments

We would like to thank the NASA Mars Fundamental Research Program (MFRP) Grant #NNG06GH18G for funding this research. Thanks to Dale Werkema and Tim Shaner for their graciousness in housing the significant amounts of field equipment required for this project. The authors would also like to thank two anonymous reviewers for their help in improving this manuscript.

References

Bierman, P., Gillespie, A., Whipple, K., Clark, D., 1991. Quaternary geomorphology and geochronology of Owens Valley, California. In: Walawender, M.J., Hanan, B.B. (Eds.), Geological Excursions in Southern California and Mexico—Guidebook 1991 Annual Meeting. Geological Society of America, Department of Geological Sciences, San Diego State University, pp. 199–223.

Blair, T.C., McPherson, J.G., 1994. Alluvial fan processes and forms. In: Abrahams, A.D., Parson, A.J. (Eds.), Geomorphology of Desert Environments. Chapman and Hall, London, pp. 354–402.

Blair, T.C., McPherson, J.G., 1998. Recent debris-flow processes and resultant form and facies of the Dolomite alluvial fan, Owens Valley, California. J. Sediment. Res. 68 (5), 800–818. September.

Blissenbach, E., 1952. Relation of surface angle distribution to particle size distribution on alluvial fans. J. Sediment. Petrol. 22, 25–28.

Boggs, S.J., 2001. Principles of Sedimentology and Stratigraphy. Prentice-Hall, Upper Saddle River, NJ.

Colwell, J.E., Jakosky, B.M., 2002. Effects of topography on thermal infrared spectra of planetary surfaces. J. Geophys. Res. 107 (E11). doi:10.1029/2001JE001829.

Gupta, R.P., 2003. Interpretation of data in the thermal-infrared region. Remote Sensing Geology. InSpringer Verlag, New York, pp. 190–203.

Jakosky, B.M., 1986. On the thermal properties of Martian fines. Icarus 66, 117–124.

Kieffer, H., Martin, T.Z., Peterfreund, A.R., Jakosky, B.M., Miner, E., Palluconi, F., 1977. Thermal and albedo mapping of Mars during the Viking primary mission. J. Geophys. Res. 82, 4249–4291.

Kraal, E., Asphaug, E., Moore, J., Howard, A., Bredt, A., 2008. Catalogue of large alluvial fans in martian impact craters. Icarus 194, 101–110.

Malin, M.C., Edgett, K.S., 2003. Evidence for persistent flow and aqueous sedimentation on early Mars. Science 302, 1931–1934.

Moore, J.M., Howard, A.D., Dietrich, W.E., Schenk, P.M., 2003. Martian layered fluvial deposits: implications for Noachian climate scenarios. Geophys. Res. Lett. 30 (24), 2292.

Pakiser, L.C., Kane, M.F., Jackson, W.H., 1964. Structural geology and volcanism of Owens Valley Region, California — a geophysical study. U.S. Geological Survey Professional Paper, vol. 438, p. 65.

Watson, K., 1975. Geologic applications of thermal infrared images. Proc. IEEE 63 (1), 128–137.

Watson, K., 1982. Regional thermal-inertia from an experimental satellite. Geophysics 47 (12), 1681–1687.

Watson, K., 2000. A diurnal animation of thermal images from a day–night pair. Remote Sens. Environ. 72, 237–243.